ChemPubSoc Europe

DOI: 10.1002/cmdc.201500479

CHEMMEDCHEM Full Papers

VIP *Very Important Paper*

SPECIAL ISSUE

Identification and Optimization of Anthranilic Acid Based Inhibitors of Replication Protein A

James D. Patrone,[a, d] Nicholas F. Pelz,[a] Brittney S. Bates,[a] Elaine M. Souza-Fagundes,[a] Bhavatarini Vangamudi,[a] Demarco V. Camper,[a] Alexey G. Kuznetsov,[a] Carrie F. Browning,[a] Michael D. Feldkamp,[a] Andreas O. Frank,[a] Benjamin A. Gilston,[a] Edward T. Olejniczak,[a] Olivia W. Rossanese,[a] Alex G. Waterson,[b, c] Walter J. Chazin,[a, c] and Stephen W. Fesik*[a, b, c]

Replication protein A (RPA) is an essential single-stranded DNA (ssDNA)-binding protein that initiates the DNA damage response pathway through protein–protein interactions (PPIs) mediated by its 70N domain. The identification and use of chemical probes that can specifically disrupt these interactions is important for validating RPA as a cancer target. A high-throughput screen (HTS) to identify new chemical entities was conducted, and 90 hit compounds were identified. From these initial hits, an anthranilic acid based series was optimized by using a structure-guided iterative medicinal chemistry approach to yield a cell-penetrant compound that binds to RPA70N with an affinity of 812 nM. This compound, 2-(3-(*N*-(3,4-dichlorophenyl)sulfamoyl)-4-methylbenzamido)benzoic acid (**20c**), is capable of inhibiting PPIs mediated by this domain.

Introduction

Replication protein A (RPA), the primary single-strand DNA (ssDNA)-binding protein in eukaryotes, is essential for DNA replication, damage response, and repair. In addition to binding to and protecting ssDNA from degradation, RPA recruits partner proteins involved in these processes. RPA is composed of three subunits, each bearing oligonucleotide/oligosaccharide-binding (OB)-fold domains.[1,2] The N-terminal domain of the 70 kDa subunit (RPA70N) is one of two key sites that mediates the recruitment of partner proteins.[3] This domain is particularly important for the recruitment of DNA damage response proteins to sites of DNA damage via interaction with the RPA70N central basic cleft.[3–6]

Based on the key role of RPA70N-mediated protein–protein interactions (PPIs) in initiating the DNA damage response, it is possible that specific inhibition of this RPA function may represent an attractive pathway for therapeutic intervention in cancer. We and others are pursuing inhibitors of the RPA70N-mediated PPIs that do not interfere with the ability of RPA to bind to and protect ssDNA, as these would allow for further exploration of the role of RPA in checkpoint signaling, enable studies to confirm the therapeutic potential of RPA inhibition, and serve as a potential starting point for new cancer drugs.

Based on this unique opportunity for small-molecule inhibitors of RPA as potential cancer therapeutics, research on RPA inhibitors has intensified over the last several years. Turchi and colleagues have identified dihydropyrazole **1** (Figure 1), which binds to a DNA-binding domain of RPA and disrupts its interaction with ssDNA.[7,8] Oakley and colleagues identified fumaropimaric acid (**2**, Figure 1), which was shown to disrupt both

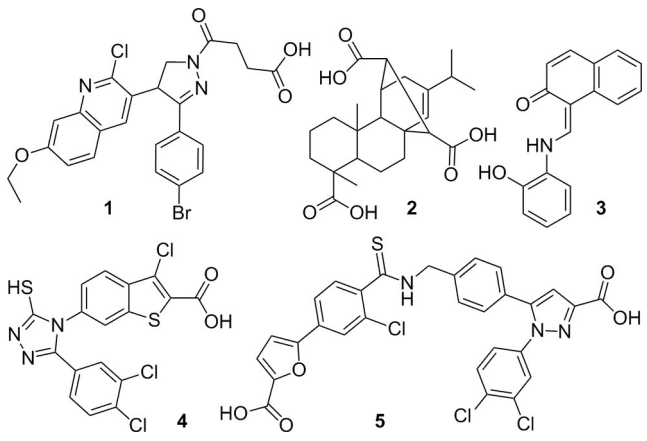

Figure 1. Previously reported RPA PPI inhibitors.

[a] *Dr. J. D. Patrone, N. F. Pelz, B. S. Bates, Prof. E. M. Souza-Fagundes, B. Vangamudi, D. V. Camper, Dr. A. G. Kuznetsov, C. F. Browning, Dr. M. D. Feldkamp, Dr. A. O. Frank, B. A. Gilston, Prof. E. T. Olejniczak, Prof. O. W. Rossanese, Prof. W. J. Chazin, Prof. S. W. Fesik*
Department of Biochemistry
Vanderbilt University, Nashville, TN 37232 (USA)
E-mail: stephen.fesik@vanderbilt.edu

[b] *Prof. A. G. Waterson, Prof. S. W. Fesik*
Department of Pharmacology
Vanderbilt University, Nashville, TN 37232 (USA)

[c] *Prof. A. G. Waterson, Prof. W. J. Chazin, Prof. S. W. Fesik*
Department of Chemistry, Vanderbilt University, Nashville, TN 37232 (USA)

[d] *Dr. J. D. Patrone*
Current address: Department of Chemistry, Rollins College, 1000 Holt Avenue, Winter Park, FL 32789 (USA)

Supporting information for this article is available on the WWW under http://dx.doi.org/10.1002/cmdc.201500479.

SPECIAL ISSUE This article is part of a Special Issue on Protein–Protein Interactions. To view the complete issue, visit: http://onlinelibrary.wiley.com/doi/10.1002/cmdc.v11.8/issuetoc.

RPA70N–Rad9 and RPA70N–p53 interactions.[9,10] The Oakley research group has also reported on HAMNO (**3**, Figure 1), which was shown to inhibit RPA binding to RAD9 and cause increased replicative stress and cytotoxicity in cancer cells and was shown to slow the progression of squamous cell carcinoma in a xenograft model.[11]

We previously reported the results of an NMR-based fragment screen to identify novel molecules that bind to RPA70N. This screen revealed several distinct chemotypes of fragments that bind to the domain. Remarkably, this single screen identified two distinct binding locations in the basic cleft of RPA70N (Site-1 and Site-2) which can be independently and simultaneously occupied by two different compounds.[12,13] From these results, we also described the results of two optimization campaigns. Initially a fragment-merging strategy was used, resulting in triazole **4** (Figure 1), which bound to only one site in the basic cleft.[12] We also described the results of a fragment-linking strategy to generate compounds that span the entire cleft and incorporate features of two distinct fragment hits (**5**, Figure 1).[13] Herein we describe a different class of molecules that was identified using a high-throughput screen (HTS) and further optimized using iterative medicinal chemistry and structure-based design.

Results and Discussion

Using a previously reported fluorescence polarization anisotropy (FPA) screening assay, 90000 compounds from the Vanderbilt collection were screened at a single concentration of 30 μM for their ability to disrupt the binding of a fluorescently labeled ATRIP-derived probe to RPA70N.[14] This screen identified 674 compounds that displaced >10% of the probe from RPA70N at this concentration. These initial hits were further filtered to remove compounds that exhibited fluorescence interference and were prioritized for follow-up on the basis of the lack of potentially reactive chemical functionality and concordance with commonly accepted measures of drug-likeness.[15,16] After this analysis, concentration–response curves were collected for 90 compounds to determine IC_{50} values, from which K_d values were calculated. Of these 90 compounds, 52 were identified with a K_d value <100 μM. Several of the most potent hits are depicted in Figure 2.[3–6]

Compound **6**, with the highest ligand efficiency (LE) amongst the hit set, was briefly investigated. The results from this work were reported previously.[17] Because of the high lipophilicity of the series and generally flat SAR, further work on the series was halted. Notably, Turchi and co-workers previously described a series of inhibitors of the interaction between RPA and ssDNA with a chemical structure similar to that of compound **9**.[17] Compounds **7** and **8** were of relatively low interest. Compounds **10** and **11** are similar and together form an anthranilic acid based series. SAR evident in the HTS hit set indicated the nitro group to be essential for binding of ether-based exemplars such as **10**. Because of this, as well as the reasonably favorable combination of potency, LE, and the prospect of a modular synthetic route, we focused follow-up efforts on sulfonamide variants such as compound **11**.

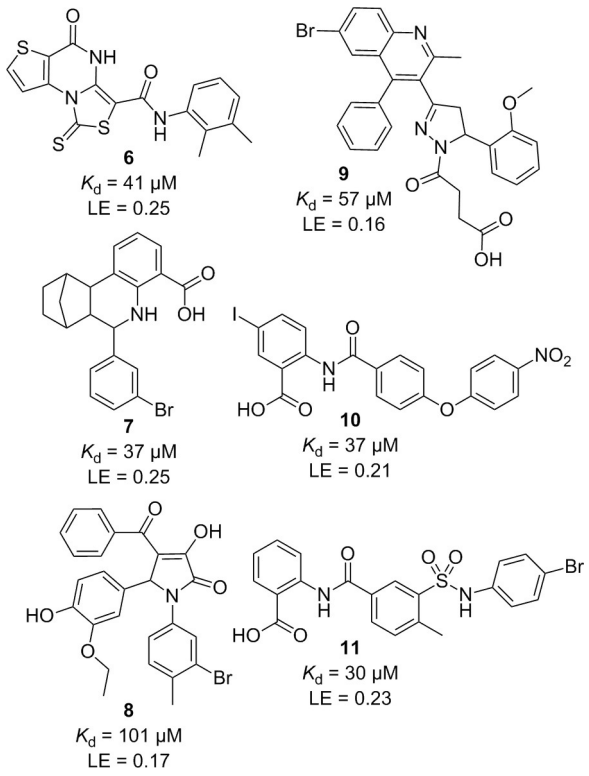

Figure 2. Selected HTS hit compounds with K_d and ligand efficiency (LE) values indicated.

To guide the optimization of **11**, a co-crystal structure of compound **11** in complex with RPA70N was obtained (Figure 3). The binding mode of compound **11** shares several important contacts with the binding mode of the p53 peptide and our previously reported molecules. The 4-bromophenyl portion of the molecule occupies the hydrophobic Site-1 pocket (Figure 3A), but lies flat against the surface of RPA70N and sits in a much more shallow position than compounds **4** and **5** (Figure 3C). The sulfonamide group of the molecule appears to establish the proper geometry necessary to orient the 4-bromophenyl into Site-1. The middle phenyl ring occupies the center of the RPA70N cleft and overlays well with the indole moiety of the tryptophan of the p53 peptide[18] (Figure 3B) or the phenylalanine of a previously reported ATRIP-derived peptide.[19] The carboxylic acid of the anthranilic acid portion of the molecule engages in a charge–charge interaction with Arg41 of RPA70N, a common interaction amongst our fragments and linked small-molecule inhibitors of RPA70N. In addition, compound **11** also makes a unique hydrogen bond interaction to Asn85 of RPA70N using the carbonyl oxygen atom of the amide bond. We hypothesized the amide in this molecule to be important owing to both this interaction with RPA and its ability to form an internal hydrogen bond with the anthranilic acid of the molecule, thus maintaining the planarity of the molecule in its binding pose.

Based on the binding mode of hit molecule **11** and our previous knowledge of small molecules binding to RPA70N, we devised a strategy to improve potency by optimizing the hydrophobic interactions of each of the phenyl rings while main-

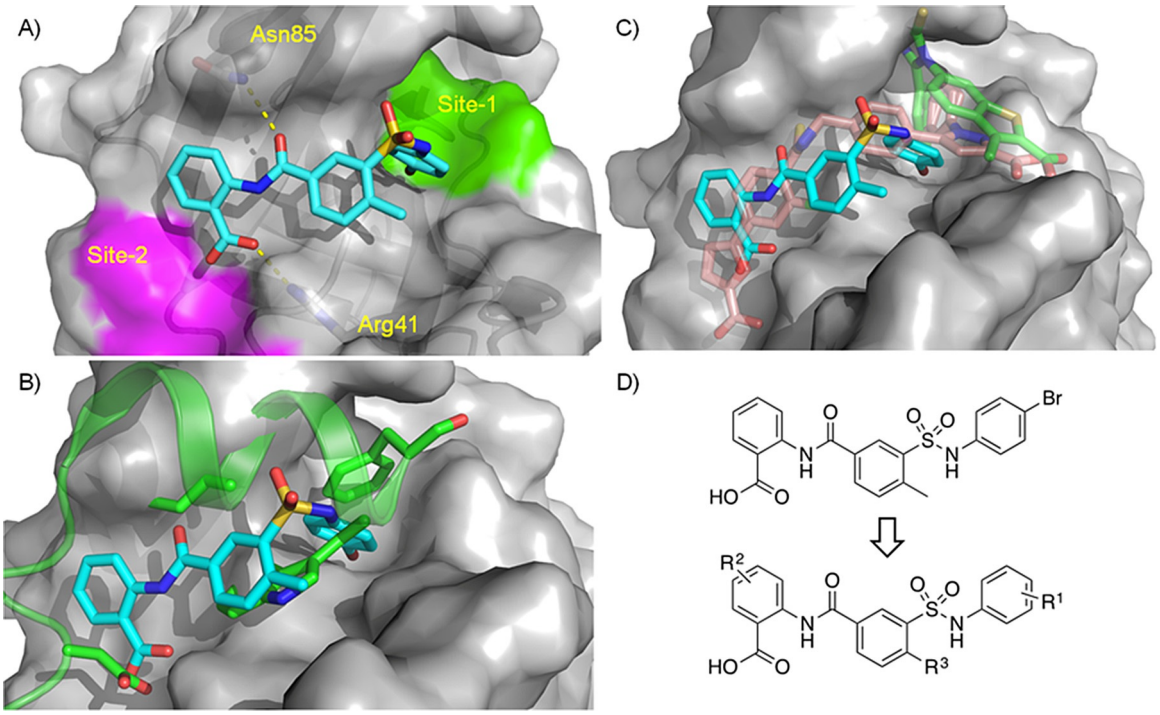

Figure 3. A) Compound **11** in complex with RPA70N. B) Compound **11** in complex with RPA70N with p53 peptide[18] superimposed. C) Compound **11** in complex with RPA70N with compounds **4** and **5** superimposed. D) SAR strategy for compound **11**.

taining the hydrophilic interactions of the amide and carboxylic acid of the molecule. The first goal was to optimize the phenyl sulfonamide portion of the molecule for binding to the hydrophobic pocket of Site-1. An initial compound library containing various phenyl substituents and phenyl replacements was constructed by using a combination of chemical synthesis and analogue purchases. Despite the majority of the analogues being less potent than the original hit, this library provided important SAR insight (Table 1).

Analogues bearing 3- or 4-chloro (**18**, **19**) were found to be equipotent with **11**, whereas non-halogen substituents such as 3-methyl, 4-methyl, or 4-methoxy (**13**, **14**, or **15**) were five- to eightfold less potent. In concordance with previously described SAR, analogue **20** (3,4-dichloro) displayed the best binding affinity of the initial set, showing a fourfold improvement over **11**. Both of the chlorine atoms are necessary, as replacing either or both with a methyl group (**21**–**23**) decreases binding affinity by six- to 20-fold relative to compound **20**. Methylation of the sulfonamide is not tolerated, as all methylated analogues were two- to fivefold less potent than the desmethyl analogues (data not shown). Replacement of the phenyl ring with saturated ring systems (compounds **27**–**32**, **34**, and **35**) in attempts to increase the hydrophobic interactions and increase the sp^3 character of the molecule, were unsuccessful, as all analogues were two- to tenfold lower in binding affinity to RPA70N. Surprisingly, the 3,4-dichloro-substituted biphenyl compound **25** was found to have an affinity (K_d) of 4 μM, despite its increased size within Site-1. However, derivatives of this molecule were not pursued further due to poor LE (0.20) and cLog*P* (6.08), as well as potential solubility limitations.

To explore the SAR around the phenyl ring of the anthranilic acid portion of the molecule, a library of analogues was synthesized with varying R^2 substituents, while R^1 was fixed as either 3,4-dichloro, 3-chloro, or 4-bromo. From this library, several clear SAR tends emerged (Table 2). Halogen R^2 options were more beneficial at the 4-position than at the 5-position, leading to an improvement of two- to tenfold. This observation can be rationalized from the co-crystal structure, in which one can envision the 5-position substituent clashing with the lip of the cleft, whereas the 4-position substituent is oriented toward a hydrophobic gap. A 5-chloro substitution at R^2 consistently led to poor physicochemical properties, such as limited solubility, as evidenced by precipitation under the assay conditions.

The most effective option at R^2 for all three different R^1 substituents was replacement of the anthranilic acid phenyl ring with a naphthyl moiety (**11l**, **18l**, and **20l**). These analogues displayed binding affinities of 1–4 μM. Based on the co-crystal structure of **11**, the naphthyl substitution most likely occupies the hydrophobic space adjacent to both the 4- and 5-positions. The analogue with the best binding affinity (**20c**), however, contained a 3,4-dichloro R^1 substitution and a 4-bromo R^2 substitution. This analogue was slightly superior to the R^2= naphthyl analogue **20l** and had a more attractive LE (0.27 compared to 0.24 for **20l**). Furthermore, compound **20c** represents the best binding affinity yet observed for a molecule with only one acidic moiety.

The final strategy to optimize compound **11** was exploration of several substituents at R^3 on the middle phenyl ring. However, several planned analogues (R^3 = chloro, bromo, or methoxy, for example) were synthetically intractable, as intermediates re-

Table 1. Structure–activity relationships in Site-1.

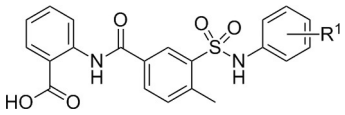

Compd	R^1	K_d [μM][a]	LE[c]
11	4-bromo	30 ± 6	0.21
12	H	156 ± 11	0.18
13	3-methyl	165 ± 34	0.18
14	4-methyl	196	0.17
15	4-methoxy	234 ± 3	0.16
16	4-ethyl	95 ± 6.5	0.18
17	4-isopropyl	76 ± 5.5	0.17
18	3-chloro	29 ± 2	0.21
19	4-chloro	44 ± 0	0.20
20	3,4-dichloro	7 ± 3	0.23
21	3,4-dimethyl	150 ± 11	0.17
22	3-chloro, 4-methyl	43 ± 3.5	0.19
23	3-methyl, 4-chloro	58 ± 11	0.18
24	2-naphthyl[b]	83 ± 8	0.17
25	3′,4′-dichloro-[1,1′-biphenyl]-3-amine[b]	4 ± 0.5	0.20
26	indane[b]	106 ± 5.5	0.17
27	cyclopentyl[b]	> 250	0.18
28	cyclohexyl[b]	193	0.18
29	4-aminotetrahydropyran[b]	> 250	n.c.[d]
30	cycloheptyl[b]	110 ± 4	0.19
31	*trans*-4-methylcyclohexyl[b]	81 ± 10	0.20
32	cyclohexylmethyl[b]	126 ± 1	0.19
33	benzyl[b]	> 250	n.c.[d]
34	azepane[b]	208	0.18
35	octahydrocyclopenta[*c*]pyrrole[b]	222 ± 28	0.17
36	isoindoline[b]	> 250	n.c.[d]

[a] Average K_d values ($n = 2$) calculated using the Cheng–Prusoff equation from IC_{50} values measured by FPA competition assay. [b] The entire ring system replaces the phenyl. [c] Ligand efficiency values calculated using LE = 1.4 × pK_d/HAC (HAC = number of non-hydrogen atoms) using FPA data. [d] Not calculated.

quired for the synthesis of these molecules were unstable under the conditions necessary for sulfonamide formation or saponification. Despite these challenges, several alkyl analogues were obtained (Table 3). The desmethyl analogue **20m** was twofold less potent than compound **20**. Further extension of the methyl to an ethyl (**20n**) or isopropyl group (**20o**) showed marginal improvements in affinity (K_d: 4 and 5 μM, respectively). However, this slight gain in potency for these analogues was offset by a decrease in solubility, with both **20n** and **20o** showing some evidence of precipitation at the highest concentrations under the assay conditions.

Using a standard fluorescence-based DNA binding assay, we established that compound **20c** does not affect ssDNA binding to RPA; the K_d value for ssDNA binding to RPA70AB in the RPA70NAB construct was the same in the absence and presence of the compound. Thus, **20c** appears to bind selectively to the RPA70N domain. Furthermore, compound **20c** was taken forward for characterization in cellular studies. The molecule was found to possess very high protein binding (99.8%), but also exhibits high permeability (P_{app} A→B value of 29.2 × 10^{-6} cm s^{-1} in the Caco-2 line) relative to our previously reported compounds. Studies to define the cellular activity of this compound are underway and will be reported in due course.

Chemistry

The synthesis of the anthranilic acid based inhibitors **11**–**36** used a modular route, allowing for the introduction of diversity at each step and only one chromatographic purification.[20] The synthesis begins with an aromatic sulfonylation, upon treating a *para*-substituted benzoic acid with chlorosulfonic acid. The carboxylic acid (compounds **40**–**42**) is converted into an acid chloride, and the methyl ester of the appropriate anthranilic acid is added to afford sulfonyl chlorides in > 90% yield (Scheme 1). After a water workup, the final substituted phenyl ring is added to the sulfonyl chloride by the addition of the appropriate substituted aniline. This is followed by saponification of the methyl ester to yield the desired analogue.

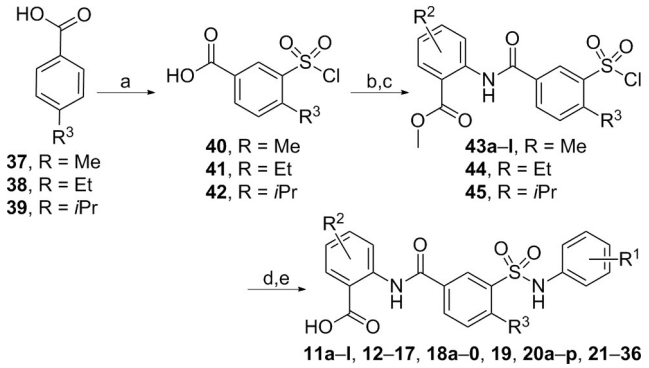

Scheme 1. General synthesis of anthranilic acid based RPA inhibitors. *Reagents and conditions*: a) chlorosulfonic acid, reflux, 16 h; b) thionyl chloride, 75 °C, 4 h; c) methyl 2-aminobenzoate–R^2, THF, 12 h; d) aniline–R^1, toluene, 70 °C, 12 h; e) 2 M LiOH, 55 °C, 2 h.

Conclusions

We conducted a high-throughput screen and initial compound optimization toward the discovery of new and selective chemical probes to validate inhibition of the protein–protein interactions mediated by RPA70N. Inhibitor **11** was initially identified as an attractive starting point for structure-based optimization. Subsequent optimization using an iterative medicinal chemistry process and structure-based design principles led to the discovery of **20c**, which binds to RPA70N with an affinity of 812 nM and displays adequate permeability and solubility characteristics for use in cellular studies.

Experimental Section

Chemistry

General methods: All chemicals, reagents, and solvents were used as purchased from commercial sources, without further purification. All NMR spectra were recorded at room temperature on a 400 MHz Bruker spectrometer with a DRX-400 console, a 500 MHz Bruker spectrometer with a DRX-500 console, or a 600 MHz Bruker spectrometer with an AV-II console. ^{1}H NMR chemical shifts (δ) are reported in ppm downfield with the deuterated solvent as the internal standard. Data are reported as follows: chemical shift, multiplicity (s = singlet, d = doublet, t = triplet, q =

Table 2. SAR of anthranilic acid ring substituents.

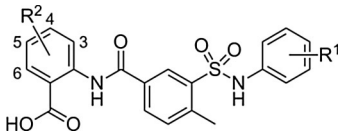

Compd	R^1	R^2	K_d [μM][a]	LE[c]	Compd	R^1	R^2	K_d [μM][a]	LE[c]
20	3,4-diCl	H	7±3	0.23	**18g**	3-Cl	5-Me	30±1	0.20
11a	4-Br	4-Cl	25±2	0.21	**18h**	3-Cl	6-Me	134±1	0.17
11b	4-Br	5-Cl	ppt[d]	n.c.[e]	**18i**	3-Cl	4,5-diMe	>250	n.c.[e]
11c	4-Br	4-Br	18±1.5	0.22	**18j**	3-Cl	5-Et	6±0.37	0.23
11d	4-Br	5-Br	20±3.5	0.21	**18k**	3-Cl	5-*i*Pr	7±0.25	0.22
11e	4-Br	4-F	34±3.5	0.20	**18l**	3-Cl	4,5-naphthyl[b]	4±0.1	0.22
11f	4-Br	5-F	48±8	0.20	**20a**	3,4-diCl	4-Cl	4±1	0.24
11g	4-Br	5-Me	33±2	0.20	**20b**	3,4-diCl	5-Cl	ppt[d]	n.c.[e]
11h	4-Br	6-Me	73±0.5	0.19	**20c**	3,4-diCl	4-Br	0.81±0.3	0.27
11i	4-Br	4,5-diMe	>250	n.c.[e]	**20d**	3,4-diCl	5-Br	8±1.3	0.22
11j	4-Br	5-Et	9±0.83	0.22	**20e**	3,4-diCl	4-F	8±2	0.22
11k	4-Br	5-*i*Pr	9±0.54	0.21	**20f**	3,4-diCl	5-F	15±1	0.21
11l	4-Br	4,5-naphthyl[b]	3±0.14	0.22	**20g**	3,4-diCl	5-Me	7±0.5	0.23
18a	3-Cl	4-Cl	8±0.45	0.23	**20h**	3,4-diCl	6-Me	36±1.5	0.19
18b	3-Cl	5-Cl	ppt[d]	n.c.[e]	**20i**	3,4-diCl	4,5-diMe	62±3.5	0.18
18c	3-Cl	4-Br	6±0.2	0.24	**20j**	3,4-diCl	5-Et	4±0.19	0.23
18d	3-Cl	5-Br	14±0.5	0.22	**20k**	3,4-diCl	5-*i*Pr	3±0.012	0.23
18e	3-Cl	4-F	22±3	0.21	**20l**	3,4-diCl	4,5-naphthyl[b]	1±0.04	0.24
18f	3-Cl	5-F	35±0	0.20					

[a] Average K_d values ($n=2$) calculated using the Cheng–Prusoff equation from IC_{50} values measured by FPA competition assay. [b] The entire ring system replaces the phenyl. [c] Ligand efficiency values calculated using LE = 1.4×pK_d/HAC (HAC = number of non-hydrogen atoms) using FPA data. [d] Visible precipitation in assay wells. [e] Not calculated.

Table 3. SAR of substituents on middle phenyl ring.

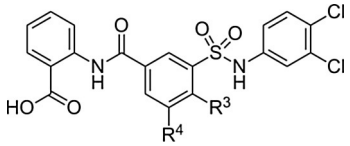

Compd	R^3	R^4	K_d [μM][a]	LE[b]
20	Me	H	7±3	0.23
20m	H	H	17±1	0.22
20n	Et	H	4±0.25[c]	0.23
20o	*i*Pr	H	5±0.19[c]	0.22
20p	Me	Me	14±1.5	0.21

[a] Average K_d values ($n=2$) calculated using the Cheng–Prusoff equation from IC_{50} values measured by FPA competition assay. [b] Ligand efficiency values calculated using LE = 1.4×pK_d/HAC (HAC = number of non-hydrogen atoms) using FPA data. [c] Some evidence of precipitation noted at highest concentrations.

quartet, br = broad, m = multiplet), coupling constant (Hz), and integration. Low-resolution mass spectra were obtained on an Agilent 1200 series 6140 mass spectrometer with electrospray ionization. All samples were of ≥90% purity as analyzed by LC–UV/Vis–MS. Analytical HPLC was performed on an Agilent 1200 series with UV detection at λ 214 and 254 nm along with ELSD detection. LC–MS parameters were as follows: Phenomenex-C_{18} Kinetex column, 50 mm×2.1 mm, 2 min gradient, 5–100% (H_2O/MeCN with 0.1% TFA). Preparative purification was performed on a Gilson HPLC (Phenomenex-C_{18}, 100 mm×30 mm, 10 min gradient, (H_2O/MeCN with 0.1% TFA) or by automated flash column chromatography (Teledyne Isco Inc., Combiflash R_f).

General procedure for anthranilic acid based inhibitors: The anthranilic acid based inhibitors **11a–l**, **12–17**, **18a–l**, **19**, **20a–p**, and **21–36** were prepared by similar procedures. This procedure is exemplified for compound **11**.[18]

3-(Chlorosulfonyl)-4-methylbenzoic acid 40: 4-Methylbenzoic acid **37** (1.0 g, 7.35 mmol, 1 equiv) was dissolved in chlorosulfonic acid (10 mL). The reaction was heated at reflux and stirred overnight. The next day, the reaction was cooled to room temperature and then poured onto ice. The solid was filtered, dissolved in CH_2Cl_2 (150 mL), and washed with 1 M HCl (50 mL). The CH_2Cl_2 layer was then dried (Na_2SO_4) and evaporated in vacuo to give the desired product **37** as a white solid (1.22 g, 71%). ^{1}H NMR (600 MHz, [D_6]DMSO): δ = 8.32 (d, J = 1.9 Hz, 1H), 7.77 (dd, J = 2.0, 7.7 Hz, 1H), 7.26 (d, J = 7.9 Hz, 1H), 2.58 ppm (s, 3H); ^{13}C NMR (125 MHz, [D_6]DMSO): δ = 167.2, 146.4, 141.2, 131.2, 129.6, 127.7, 127.5, 20.3 ppm; MS (ESI) $[M+H]^+$ m/z = 234.9.

Methyl 2-(3-(chlorosulfonyl)-4-methylbenzamido)benzoate 43a: The intermediate **40** (235 mg, 1 mmol, 1 equiv) was dissolved in thionyl chloride (4 mL). The reaction was heated at 75 °C and stirred for 4 h. Solvents were removed in vacuo. The resulting syrup was dissolved in toluene (3×5 mL) and evaporated. The product was taken forward without further purification. The appropriate methyl-2-aminobenzoate (151 mg, 1 mmol, 1 equiv) was dissolved in THF (4 mL), and NaH (40 mg, 1 mmol, 1 equiv) was added and stirred for 20 min. The acyl chloride (1 mmol, 1 equiv) was added, and the reaction was stirred at RT for 2 h. The reaction was diluted with CH_2Cl_2 (100 mL) and washed with water (25 mL). The CH_2Cl_2 layer was dried (Na_2SO_4) and then evaporated in vacuo. The white solid residue was taken forward without further purification (367 mg, quant). ^{1}H NMR (600 MHz, [D_6]DMSO): δ = 8.57 (dd, J = 0.8, 8.5 Hz, 1H), 8.39 (d, J = 2.1 Hz, 1H), 8.00 (dt, J = 1.9, 8.0 Hz, 1H), 7.80 (dd, J = 2.1, 7.8 Hz, 1H), 7.67 (m, 1H), 7.37 (d, J = 7.9 Hz, 1H),

7.22 (m, 1H), 3.90 (s, 3H), 2.62 ppm (s, 3H); ^{13}C NMR (150 MHz, [D$_6$]DMSO): δ = 168.0, 164.7, 146.9, 140.5, 140.3, 134.3, 131.4, 131.1, 130.8, 127.0, 125.7, 123.3, 120.9, 117.1, 52.7, 20.2 ppm; MS (ESI) $[M+H]^+$ m/z = 368.0.

2-(3-(*N*-(4-Bromophenyl)sulfamoyl)-4-methylbenzamido)benzoic acid 11: The sulfonyl chloride **43a** (62 mg, 0.17 mmol, 1 equiv) was dissolved in toluene (2 mL). The 4-bromoaniline (86 mg, 0.5 mmol, 3 equiv) was added, and the reaction was stirred at 70 °C overnight. The solvents were removed in vacuo. The resulting residue was dissolved in CH_2Cl_2 (50 mL) and washed with water (20 mL). The CH_2Cl_2 layer was evaporated in vacuo, and the residue was dissolved in THF (2 mL), and 2 M LiOH (0.5 mL) was added. The reaction was stirred at 55 °C for 2 h. The reaction was neutralized with 2 M HCl (0.5 mL), and the solvents were removed in vacuo. The residue was purified by preparative HPLC to give the desired product as a white solid (23 mg, 28%). ^{1}H NMR (600 MHz, [D$_6$]DMSO): δ = 10.78 (s, 1H), 8.67 (dd, J = 0.8, 8.4 Hz, 1H), 8.52 (d, J = 1.9 Hz, 1H), 8.08–8.05 (m, 2H), 7.68 (m, 1H), 7.62 (d, J = 8.1 Hz, 1H), 7.43–7.41 (m, 2H), 7.24 (m, 1H), 7.09–7.06 (m, 2H), 3.39 (br s, 1H), 2.66 ppm (s, 3H); ^{13}C NMR (150 MHz, [D$_6$]DMSO): δ = 170.6, 163.5, 141.6, 141.3, 138.3, 137.1, 134.9, 134.1, 133.0, 132.7, 131.9, 131.8, 128.7, 123.8, 121.5, 120.5, 117.2, 116.2, 20.2 ppm; MS (ESI) $[M+H]^+$ m/z = 489.1.

2-(3-(*N*-(3-Chlorophenyl)sulfamoyl)-4-methylbenzamido)benzoic acid 18: Synthesized as a white solid according to procedure for **11** in 42% yield (29 mg). ^{1}H NMR (600 MHz, [D$_6$]DMSO): δ = 10.88 (s, 1H), 8.67 (dd, J = 0.9, 8.4 Hz, 1H), 8.55 (d, J = 1.9 Hz, 1H), 8.09–8.06 (m, 2H), 7.68 (m, 1H), 7.63 (d, J = 8.1 Hz, 1H), 7.27–7.23 (m, 2H), 7.12–7.09 (m, 2H), 7.04 (m, 1H), 3.40 (br s, 1H), 2.67 ppm (s, 3H); ^{13}C NMR (150 MHz, [D$_6$]DMSO): δ = 170.1, 162.9, 141.2, 140.7, 138.8, 137.8, 134.4, 133.6, 133.5, 132.5, 132.4, 131.4, 131.3, 131.1, 128.2, 123.4, 123.3, 120.0, 118.1, 116.9, 19.7 ppm; MS (ESI) $[M+H]^+$ m/z = 445.2.

4-Bromo-2-(3-(*N*-(3-chlorophenyl)sulfamoyl)-4-methyl benzamido)benzoic acid 18c: Synthesized as a white solid according to procedure for **11** in 34% yield (28 mg). ^{1}H NMR (600 MHz, [D$_6$]DMSO): δ = 10.91 (s, 1H), 8.93 (d, J = 2.0 Hz, 1H), 8.55 (d, J = 2.0 Hz, 1H), 8.06 (dd, J = 1.8, 7.4 Hz, 1H), 7.99 (d, J = 8.4 Hz, 1H), 7.63 (d, J = 8.0 Hz, 1H), 7.44 (dd, J = 2.0, 8.6 Hz, 1H), 7.27 (t, J = 8.1 Hz, 1H), 7.13–7.10 (m, 2H), 7.05 (m, 1H), 3.42 (br s, 1H), 2.68 ppm (s, 3H); ^{13}C NMR (150 MHz, [D$_6$]DMSO): δ = 168.0, 161.5, 140.1, 139.8, 137.1, 136.2, 132.1, 131.9, 131.3, 130.3, 129.8, 129.5, 126.6, 126.1, 124.5, 121.8, 120.6, 116.5, 115.2, 114.2, 18.1 ppm; MS (ESI) $[M+H]^+$ m/z = 568.9.

4-Bromo-2-(3-(*N*-(3,4-dichlorophenyl)sulfamoyl)-4-methyl benzamido)benzoic acid 20c: Synthesized as a white solid according to procedure for **11** in 42% yield (34 mg). ^{1}H NMR (600 MHz, [D$_6$]DMSO): δ = 11.05 (s, 1H), 8.92 (d, J = 2.1 Hz, 1H), 8.53 (d, J = 1.9 Hz, 1H), 8.06 (dd, J = 1.9, 7.9 Hz, 1H), 7.98 (d, J = 8.5 Hz, 1H), 7.64 (d, J = 8.2 Hz, 1H), 7.50 (d, J = 8.8 Hz, 1H), 7.43 (dd, J = 2.1, 8.5 Hz, 1H), 7.28 (d, J = 2.6 Hz, 1H), 7.12 (dd, J = 2.6, 8.9 Hz, 1H), 3.39 (br s, 1H), 2.67 ppm (s, 3H); ^{13}C NMR (150 MHz, [D$_6$]DMSO): δ = 169.6, 163.1, 141.8, 141.5, 137.6, 137.4, 133.8, 133.0, 132.1, 131.6, 131.6, 131.4, 128.2, 127.7, 126.1, 125.6, 122.2, 119.8, 118.3, 115.8, 19.7 ppm; MS (ESI) $[M+H]^+$ m/z = 556.9.

Fluorescence polarization anisotropy (FPA) assays

90 000 compounds from the Vanderbilt Institute of Chemical Biology compound collection were screened at the High-Throughput Screening core at a single concentration of 30 μM for their ability to disrupt the binding of an ATRIP-based probe to RPA70N. The protocol is described in full detail in the report by Souza-Fagundes et al.[14] FPA competition assays were conducted as previously described with minor modifications.[12,14] Compounds were diluted in a ten-point, threefold serial dilution scheme in DMSO for a final concentration range of 500–0.025 μM. Compounds were added to assay buffer (50 mM HEPES, 75 mM NaCl, 5 mM DTT, pH 7.5) containing FITC-labeled probe and appropriate RPA70 protein in a final reaction volume of 50 μL containing 5% DMSO. All assays were conducted using a protein concentration equal to 1 × K_d for the protein–probe interaction. Therefore, competition for binding to RPA70N was measured using either the FITC-ATRIP peptide (FITC-Ahx-DFTADDLEELDTLAS-NH$_2$; 50 nM with 6 μM RPA70N) or the FITC-ATRIP2 peptide (FITC-Ahx-DFTADDLEEWFAL-NH$_2$; 25 nM with 350 nM RPA70N). Binding to RPA70NAB was measured using 200 nM RPA70NAB and 25 nM FITC-ATRIP2. Following incubation for 1 h, emission anisotropy was measured using an EnVision plate reader (PerkinElmer). IC_{50} values were generated using a four-parameter dose–response (variable slope) equation in XLfit and were converted into K_d values. Reported K_d values are the average of two independent experiments, run in duplicate.

X-ray crystal structures of complexes with RPA70N

Crystals of the E7R mutant of RPA70N were grown as described previously.[21] X-ray diffraction data were collected at sector 21 (Life Sciences Collaborative Access Team, LS-CAT) of the Advanced Photon Source (Argonne, IL, USA). All data were processed by HKL-2000.[22] E7R crystallized in space group $P2_12_12_1$ and contained one molecule in the asymmetric unit. Initial phases were obtained by molecular replacement with PHASER[23] using the structure of the free protein (PDB ID: 4IPC) as a search model. Iterative cycles of model building and refinement were performed using COOT[24] and PHENIX.[25] The structure of compound **20c** bound to E7R are deposited at the RCSB Protein Data Bank under accession code 5E7N. The program PyMOL (Schrödinger) was used to visualize and analyze the structures.

Protein binding and cellular permeability studies

The studies on **20c** were performed by Absorption Systems, a preclinical contract research organization. Brief details of the studies can be found in the Supporting Information.

Acknowledgements

We thank Dr. David Cortez (Vanderbilt University Department of Biochemistry) for his intellectual contributions in the conception of this project. We also acknowledge the Vanderbilt High-Throughput Screening Core, an institutionally supported facility in which some of these experiments were performed and whose staff provided invaluable assistance. Funding of this research was provided in part by US National Institutes of Health (NIH) grants 5DP1OD006933/8DP1A174419 (NIH Director's Pioneer Award) to S.W.F., R01M065484 and P01CA092584 to W.J.C., and an American Recovery and Reinvestment Act (ARRA) stimulus grant (5RC2A148375) to Lawrence J. Marnett, as well as funding from the Brazilian National Council for Scientific and Technological Development (CNPq) and the Federal University of Minas Gerais (Brazil) to E.M.S.-F. A.O.F. was supported by a postdoctoral fellow-

ship from the Deutscher Akademischer Austauschdienst (DAAD), J.D.P. by an NIH National Research Service Award (NRSA) postdoctoral fellowship (F32CA174315-02), and M.D.F. by an NIH NRSA postdoctoral fellowship (F32ES021690-01).

Keywords: high-throughput screening · hit optimization · medicinal chemistry · protein–protein interactions · replication protein A

[1] M. S. Wold, *Annu. Rev. Biochem.* **1997**, *66*, 61.
[2] M. S. Wold, T. Kelly, *Proc. Natl. Acad. Sci. USA* **1988**, *85*, 2523.
[3] X. Xu, S. Vaithiyalingam, G. G. Glick, D. A. Mordes, W. J. Chazin, D. Cortez, *Mol. Cell. Biol.* **2008**, *28*, 7345.
[4] E. Fanning, V. Klimovich, A. R. Nager, *Nucleic Acids Res.* **2006**, *34*, 4126.
[5] D. Cortez, S. Guntuku, J. Qin, S. J. Elledge, *Science* **2001**, *294*, 1713.
[6] K. A. Cimprich, D. Cortez, *Nat. Rev. Mol. Cell Biol.* **2008**, *9*, 616.
[7] B. J. Andrews, J. J. Turchi, *Mol. Cancer Ther.* **2004**, *3*, 385.
[8] S. C. Shuck, J. J. Turchi, *Cancer Res.* **2010**, *70*, 3189.
[9] J. G. Glanzer, S. Q. Liu, G. G. Oakley, *Bioorg. Med. Chem.* **2011**, *19*, 2589.
[10] J. G. Glanzer, K. A. Carnes, P. Soto, S. Liu, L. J. Parkhurst, G. G. Oakley, *Nucleic Acids Res.* **2013**, *41*, 2047.
[11] J. G. Glanzer, S. Liu, L. Wang, A. Mosel, A. Peng, G. G. Oakley, *Cancer Res.* **2014**, *74*, 5165.
[12] J. D. Patrone, J. P. Kennedy, A. O. Frank, M. D. Feldkamp, B. Vangamudi, N. F. Pelz, O. W. Rossanese, A. G. Waterson, W. J. Chazin, S. W. Fesik, *ACS Med. Chem. Lett.* **2013**, *4*, 601.
[13] A. O. Frank, M. D. Feldkamp, J. P. Kennedy, A. G. Waterson, N. F. Pelz, J. D. Patrone, B. Vangamudi, D. V. Camper, O. W. Rossanese, W. J. Chazin, S. W. Fesik, *J. Med. Chem.* **2013**, *56*, 9242.
[14] E. M. Souza-Fagundes, A. O. Frank, M. D. Feldkamp, D. C. Dorset, W. J. Chazin, O. W. Rossanese, E. T. Olejniczak, S. W. Fesik, *Anal. Biochem.* **2012**, *421*, 742.
[15] J. B. Baell, G. A. Holloway, *J. Med. Chem.* **2010**, *53*, 2719.
[16] C. A. Lipinski, F. Lombardo, B. W. Dominy, P. J. Feeney, *Adv. Drug Delivery Rev.* **1997**, *23*, 3.
[17] V. J. Anciano Granadillo, J. N. Earley, S. C. Shuck, M. M. Georgiasdis, R. W. Fitch, J. J. Turchi, *J. Nucleic Acids* **2010**, 1.
[18] E. Bochkareva, L. Kasutov, A. Ayed, G.-S. Yi, A. Pineda-Lucena, J. C. C. Liao, A. L. Okorokov, J. Milner, C. H. Arrowsmith, A. Bochkarev, *Proc. Natl. Acad. Sci. USA* **2005**, *102*, 15412.
[19] A. O. Frank, B. Vangamudi, M. D. Feldkamp, E. M. Souza-Fagundes, J. W. Luzwick, D. Cortez, E. T. Olejniczak, A. G. Waterson, O. W. Rossanese, W. J. Chazin, S. W. Fesik, *J. Med. Chem.* **2014**, *57*, 2455.
[20] A. Thorarensen, C. J. Ruble, D. L. Romero (Pfizer Inc.), Int. PCT Pub No. WO 2004018428 A3, **2004**.
[21] M. D. Feldkamp, A. O. Frank, J. P. Kennedy, J. D. Patrone, B. Vangamudi, A. G. Waterson, S. W. Fesik, W. J. Chazin, *Biochemistry* **2013**, *52*, 6515.
[22] Z. M. Otwinowski, W. Minor, *Methods Enzymol.* **1997**, *276*, 307.
[23] M. D. Winn, C. C. Ballard, K. D. Cowtan, E. J. Dodson, P. Emsley, P. R. Evans, R. M. Keegan, E. B. Krissinel, A. G. Leslie, A. McCoy, S. J. McNicholas, G. N. Murshudov, N. S. Pannu, E. A. Potterton, H. R. Powell, R. J. Read, A. Vagin, K. S. Wilson, *Acta Crystallogr. Sect. D* **2011**, *67*, 235.
[24] P. Emsley, K. Cowtan, *Acta Crystallogr. Sect. D* **2004**, *60*, 2126.
[25] P. D. Adams, P. V. Afonine, G. Bunkoczi, V. B. Chen, I. W. Davis, N. Echols, J. J. Headd, L. W. Hung, G. J. Kapral, R. W. Grosse-Kunstleve, A. J. McCoy, N. W. Moriarty, R. Oeffner, R. J. Read, D. C. Richardson, J. S. Richardson, T. C. Terwilliger, P. H. Zwart, *Acta Crystallogr. Sect. D* **2010**, *66*, 213.

Received: October 14, 2015
Revised: December 8, 2015
Published online on January 8, 2016